ELSEVIER

Journal of Atmospheric and Solar-Terrestrial Physics 70 (2008) 245–253

Journal of ATMOSPHERIC AND SOLAR-TERRESTRIAL PHYSICS

www.elsevier.com/locate/jastp

Solar sources and geospace consequences of interplanetary magnetic clouds observed during solar cycle 23

N. Gopalswamy[a,*], S. Akiyama[a,b], S. Yashiro[a,b], G. Michalek[a,b], R.P. Lepping[a]

[a]*NASA Goddard Space Flight Center, Code 695.0, Greenbelt, MD 20771, USA*
[b]*Department of Physics, The Catholic University of America, 200 Hannan Hall, Washington, DC 20064, USA*

Accepted 27 August 2007
Available online 9 October 2007

Abstract

We present results of a statistical investigation of 99 magnetic clouds (MCs) observed during 1995–2005. The MC-associated coronal mass ejections (CMEs) are faster and wider on the average and originate within $\pm 30^{\circ}$ from the solar disk center. The solar sources of MCs also followed the butterfly diagram. The correlation between the magnetic field strength and speed of MCs was found to be valid over a much wider range of speeds. The number of south–north (SN) MCs was dominant and decreased with solar cycle, while the number of north–south (NS) MCs increased confirming the odd-cycle behavior. Two-thirds of MCs were geoeffective; the Dst index was highly correlated with speed and magnetic field in MCs as well as their product. Many (55%) fully northward (FN) MCs were geoeffective solely due to their sheaths. The non-geoeffective MCs were slower (average speed $\sim$382 km/s), had a weaker southward magnetic field (average ~ -5.2 nT), and occurred mostly during the rise phase of the solar activity cycle.

Keywords: Coronal mass ejections; Magnetic clouds; Space weather; Solar cycle

1. Introduction

Parker (1957) used the term magnetic cloud (MC) to denote a hydromagnetic gas cloud with tangled magnetic field ejected from the Sun. Currently MC denotes an interplanetary (IP) structure with enhanced magnetic field strength, smooth rotation of the magnetic field and a low plasma beta (Burlaga et al., 1981). There have been several investigations of MCs in the past mainly concentrated on the statistical properties and geoeffectiveness (see Lepping et al., 2005; Echer et al., 2005; Huttunen et al., 2005 and references therein). Here we focus on both the solar origin and geoeffectiveness of MCs observed over solar cycle 23 (1995–2005). The solar source of an MC is defined as the associated white light coronal mass ejection (CME). MCs form a subset of interplanetary CMEs (ICMEs). An ICME is considered to be geoeffective (GE) if the associated Dst index is $\leqslant 50$ nT. According to Loewe and Prölss (1997), a geomagnetic storm can be intense ($\mathrm{Dst} \leqslant -100$ nT), moderate (-100 nT $<$ Dst $\leqslant -50$ nT), and weak (Dst > -50 nT). While the moderate and weak storms may be caused by both CIRs and ICMEs, the intense ones are mostly

*Corresponding author. Tel.: +1 301 286 5885; fax: +1 301 286 1433.
E-mail address: gopals@ssedmail.gsfc.nasa.gov (N. Gopalswamy).

1364-6826/$ - see front matter © 2007 Elsevier Ltd. All rights reserved.
doi:10.1016/j.jastp.2007.08.070

caused by ICMEs (Gosling et al., 1991). Since the southward component of ICME magnetic field primarily decides the geoeffectiveness, we investigate the internal magnetic structure of MCs and their sheaths.

2. Data and MC properties

We considered the MCs listed in the Wind Magnetic Field Investigation (MFI, Lepping et al., 1995) web site.[1] We also use two MCs from the Advanced Composition Explorer (ACE) detected during the Halloween 2003 period (Gopalswamy et al., 2005) when Wind was not located in the solar wind. The list of 99 MCs are given in the electronic supplement with the following sets of information: (i) properties of MCs (columns 1–11), (ii) date, time, and speed of the associated IP shocks (columns 12–14), (iii) date, start time, and strength of the associated geomagnetic storms (columns 15–18), and (iv) date, time, width, speed, and solar source location of the associated CMEs as observed by the Solar and Heliospheric Observatory (SOHO) mission's Large Angle and Spectrometric Coronagraphs (LASCO) in columns 19–22. The date, onset time, duration, and speed of MCs were taken from the MFI web site. The maximum field strength (Bt in nT) and the southward component (Bz in nT in GSE coordinates) were obtained from the Omniweb.[2] Both the maximum magnitude of Bz (|Bz|max) and the minimum value of Bz (Bzmin) are listed. The numbers in parentheses for Bt, |Bz|max, Bzmin, and Dst correspond to sheaths of MCs. For shock-driving CMEs, the sheaths correspond to the region between the shock and the MC onset; for MCs without shocks, we list the above quantities in a 12-h interval preceding the MC onset for reference. The solar source location is identified with the heliographic coordinates of the associated H-alpha or soft X-ray flare as listed in the online Solar Geophysical Data (SGD). If locations are not listed, we used movies of EUV (SOHO), soft X-ray (Yohkoh), or microwave (Nobeyama radioheliograph) images to identify the associated eruption from one or more of the following signatures: coronal dimming, filament eruption, and post-eruption arcade formation. We used IP shocks listed in the SOHO/CELIAS web site.[3] Properties of SOHO/LASCO CMEs are from the online catalog.[4]

From the electronic table, we see that the average values of Bt (18 nT) and Bz (9.4 nT) are much higher than the corresponding solar wind values at 1 AU. The duration of MCs ranges from a few hours to more than 40 h with an average value of 20.5 h (see Lepping et al., 2006 for details on MC properties). The mean speed of MCs (487 km/s) is slightly higher than that of the slow solar wind (440 km/s). The MC-associated CMEs had much higher average speed (774 km/s), but smaller than the average speed of halo CMEs (1052 km/s) and GE CMEs (1042 km/s). The smaller average speed for MC-related CMEs may be due to projection effects. In fact, the average speed of MC-related CMEs is much closer to the halo CMEs originating close to the disk center (see Gopalswamy et al., 2007). The MC-associated CMEs were mostly halos (63%); 86% had width $\geqslant 120^{\circ}$. The average width of 10 non-halos is 71°, much larger than that of the general population (see e.g., Gopalswamy, 2006).

The speeds of CMEs (V_{CME}) and MCs (V_{MC}) are related to the MC magnetic fields (Bt, Bz) as shown in Fig. 1. The V_{MC}–Bt correlation is the highest, but the coefficient ($r = 0.56$) is significantly different from 0.75 obtained by Gonzalez et al. (1998) for a smaller set (30 MCs) and 0.35 obtained by Echer et al. (2005) for a larger set (149 MCs). These authors used peak MC speed, but we use the average MC speed in order to eliminate the expansion speed of the clouds; our results also correspond to a wider range of MC speeds by a factor of 2. Our results do not agree with those of Owens et al. (2005), who used only 30 MCs for the detailed analysis. These authors suggested that the peak speed of MCs used by Gonzalez et al. (1998) might reflect the sheath speed. Such an explanation does not apply to our MCs because we use average speeds rather than peak speeds. The V_{MC}–Bz correlation is even weaker ($r = 0.34$). When the two high-speed outliers in Fig. 1(b) and (d) are eliminated, the correlation improves slightly: $r = 0.59$ for V_{MC}–Bt and 0.43 for V_{MC}–Bz. The V_{CME}–Bt correlation is also positive but weak ($r = 0.40$); the scatter plot is similar to that of Lindsay et al. (1999), who did not separate MCs from non-cloud (NC) ICMEs; their data also correspond to a different heliocentric distance (~0.7 AU). Since CMEs are magnetically driven, the correlation between V_{CME} and Bt is significant because the solar source region magnetic field erupts

[1] http://lepmfi.gsfc.nasa.gov/mfi/mag_cloud_S1.html.
[2] http://omniweb.gsfc.nasa.gov.
[3] http://umtof.umd.edu/pm/FIGS.html.
[4] http://cdaw.gsfc.nasa.gov/CME_list.

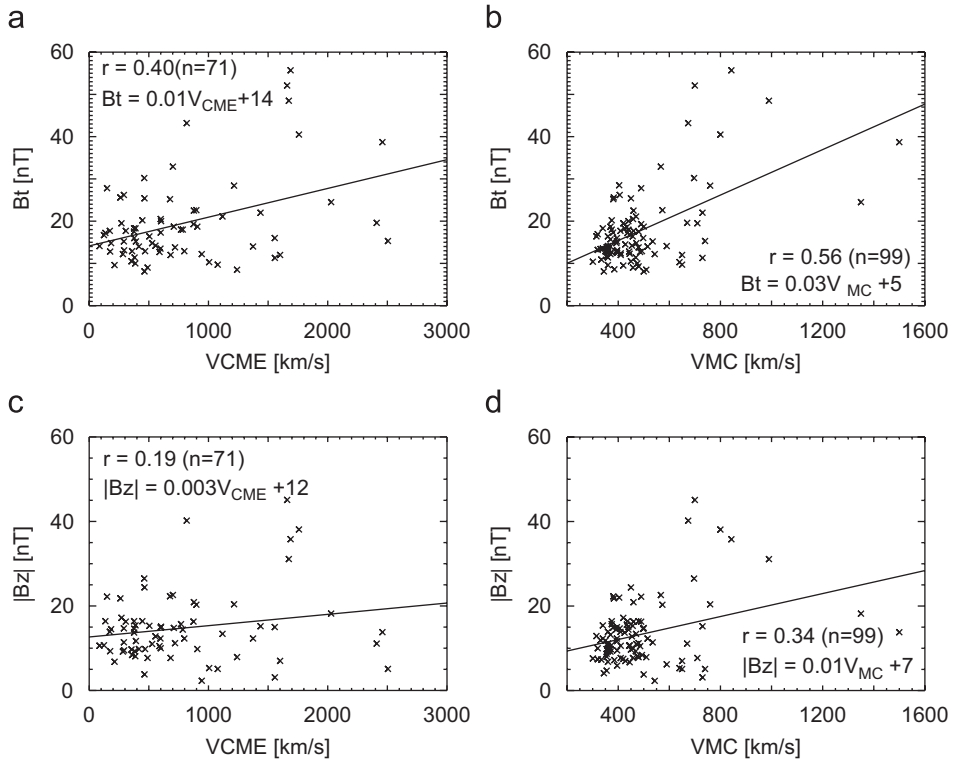

Fig. 1. Scatter plots showing how CME (left) and MC (right) speeds relate to the MC magnetic fields. Maximum |Bz| values are used because some MCs had only northward field. The number of events (n), correlation coefficient (r) and the equation of the regression line are given on the plots.

and eventually becomes the MC magnetic field. The V_{CME}–Bz correlation is also positive but very poor ($r = 0.19$). Much better correlation was claimed by Yurchyshyn et al. (2004) for a set of 14 ICMEs (only six were MCs), and the correlation was made between ICME speed and the Bz in the ICME or sheath, whichever was larger.

3. Solar sources of MCs

Fig. 2(a) shows the heliographic locations of the MC-associated CMEs, with the three phases of the solar cycle distinguished. The MC sources are clustered close to the disk center, 96% of them lying within $\pm 30^\circ$ latitude. Similarly, 91% of the sources are located within $\pm 30^\circ$ longitude. The outliers in latitude are all from the rise phase of the solar cycle. Sixty eight MCs (69%) were preceded by IP shocks, as listed in the electronic table. In Fig. 2(b), we compare the sources of shock-driving MCs with those of shock-driving non-cloud (NC) ejecta, and shocks (S) without drivers. The NC sources are scattered over a much wider longitude range. The S sources are generally closer to the limb. The distributions suggest that CMEs in the MC and S events are ejected along and orthogonal to the Sun–Earth line, respectively. The NC sources correspond to CMEs ejected at intermediate angles. The nature of the IP structure seems to be decided by the location of eruption on the Sun, supporting the view that all ejecta may be MCs if viewed from suitable vantage points. However, some shock and NC sources are located close to the disk center. In these cases, other factors such as deflection of CMEs by other CMEs or coronal holes, narrower CMEs, and unfavorable solar B-angle need to be considered.

The average longitude of MC sources is W07, while the latitude distribution is bimodal, corresponding to the active region belts on either side of the equator (see Fig. 3). The average latitudes are S19 and N16 in the southern and northern hemispheres, respectively. In the rise (1996–1998), maximum (1999–May 2002) and declining (June 2002–2005) phases of the solar cycle, the longitudes

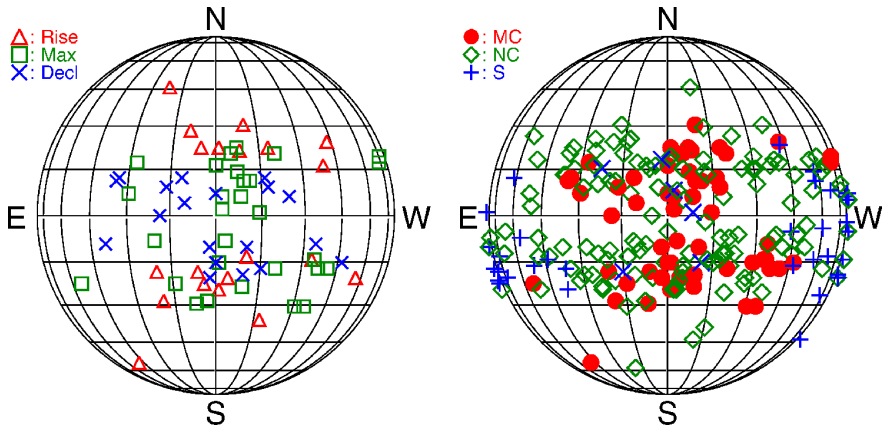

Fig. 2. (left) Heliographic locations of MC-associated CMEs during the rise (1996–1998, triangles), maximum (1999–May 2002, squares), and declining (May 2002–2005, crosses) phases of the solar cycle. (right) Solar sources of CMEs associated with interplanetary shocks driven by MCs (circles), non-cloud ejecta (NC, diamonds) and "driverless" shocks (S, plus symbols and crosses) (right). The shocks represented by crosses are associated with narrower CMEs, which might explain why the shock driver did not arrive at Earth.

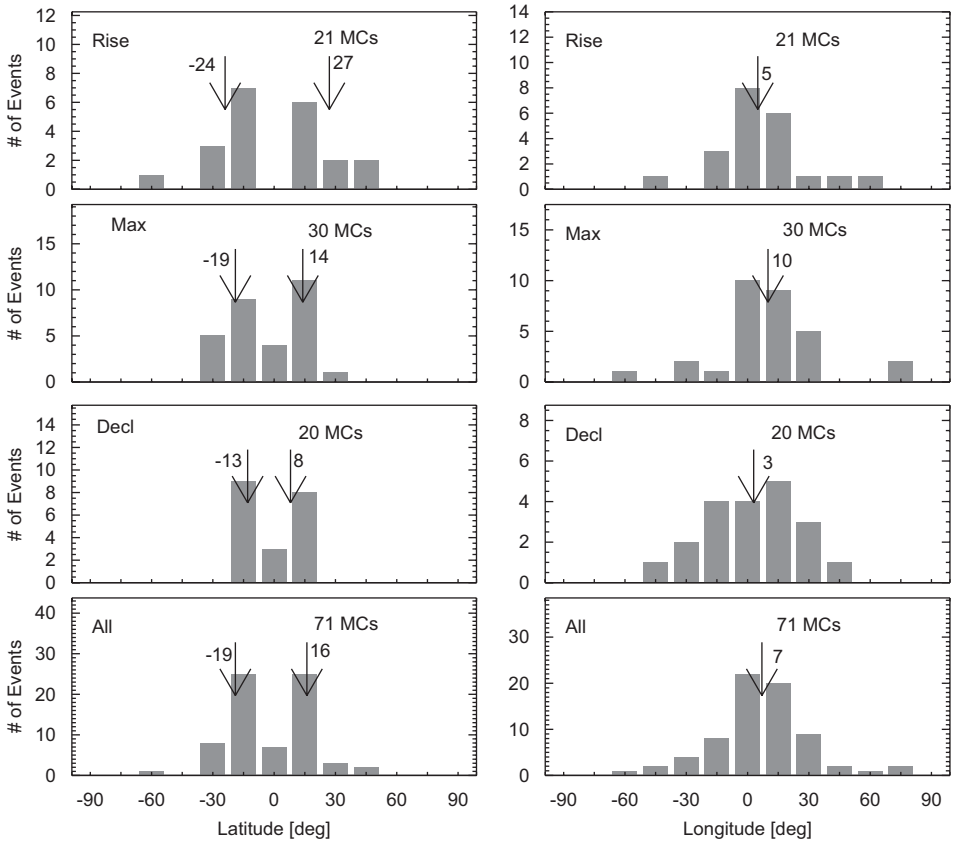

Fig. 3. The latitude (left) and longitude (right) distributions of MCs during the three phases of cycle 23 and for all MCs (bottom panel). Note the narrowing of the latitude distributions as one goes from the rise to the declining phases. The longitudinal spread is slightly higher during the maximum phase. The maximum phase is extended to May 2002 taking the completion of solar polarity reversal into consideration. The averages of the distributions are marked on the plots (shown separately for north and south for latitude distributions).

are quite similar, averaging W05, W10, and W03, respectively. The latitude distribution narrows as one goes from the rise (N27, S24) to the maximum (N14, S19) to the declining (N08, S13) phases. There are no sources at very low latitudes during the rise phase because active regions generally originate at

relatively higher latitudes in the beginning of the cycle.

Fig. 4 shows that during the maximum and declining phases, the sources are much closer to the equator than in the rise phase, resembling the butterfly diagram (there is a clear trend of decreasing uppermost latitude in both hemispheres as the solar cycle progresses from solar minimum). Even though MCs during the rise phase originate from higher latitudes, their arrival at Earth is probably due to the global dipolar field of the Sun, which is strong in this phase and guides the CMEs towards the equator (Gopalswamy et al., 2000, 2003a). While there are roughly the same numbers of MCs originating from the northern and southern hemispheres over the study period, there is some asymmetry over shorter time scales. There is a dearth of MCs during 1999 in both hemispheres and another interval of no MCs from the northern hemisphere during 2002–2004.

Also shown in Fig. 4 is the solar cycle variation of the MC types classified based on how the southward component of the magnetic field changes direction from the front to back of the MC: south–north (SN), fully south (FS), north–south (NS), fully north (FN). We used a very simple criterion to classify the magnetic structure: if 90% of the MC interval has continuous southward (northward) Bz in GSE coordinates, we regarded it as an FS (FN) MC. This simple criterion works for most of the MCs because the By component shows a smooth east–west rotation. If this simple criterion is not satisfied, the MC is either SN or NS depending on the leading field. For five FN MCs, the Bz shows 100% northward, but the rotation in the y-direction is not clear, so we retained them as FN clouds. The cloud fitting to these MCs was also of poor quality. Table 1 shows that SN clouds were the largest in number (39 out of 99 or 39%) during cycle 23, which is roughly two times the numbers in each of the other types (FS—19 (19%) , NS—21 (21%), and FN—20 (20%)).

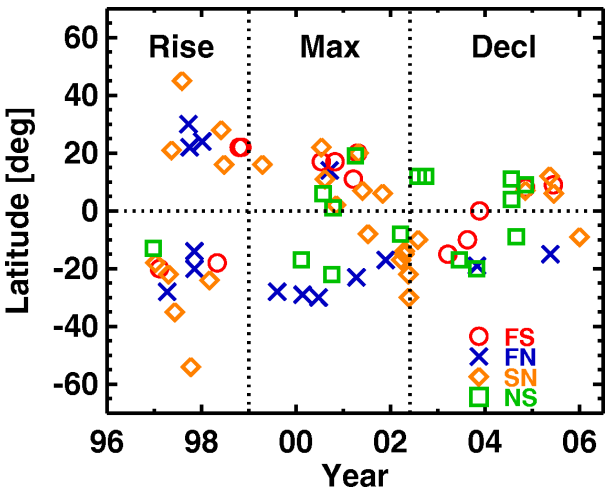

Fig. 4. Time evolution of solar source latitudes of MCs. The three phases of the solar cycle (Rise, Max, Decl.) are delineated by the vertical dashed lines. The four types of MCs are distinguished: fully south (FS), fully north (FN), south–north (SN) and north–south (NS) clouds. The number of MCs in each cloud type in the rise, maximum, and declining phases: 4,7,10 (NS); 19, 15, 5 (SN); 9,7,4 (FN); 8,5,6 (FS). The monotonic decrease in MC latitudes from the minimum to declining phases is evident. The control of the solar global field decreases from solar minimum to maximum, which might explain why CMEs originating close to 50° latitude can arrive at 1 AU as MCs.

The number of SN clouds monotonically declines from the rise phase (19) to the maximum phase (15) and then to the declining phase (5). The number of FS MCs remains virtually the same in the three phases (8, 5, 6), while the number of FN MCs shows a decrease (9, 7, 4). The NS is the only MC type showing an increasing trend (4, 7, 10). The predominance of SN MCs over the NS MCs and their opposite trend in occurrence rate are consistent with what is expected for odd cycles (Mulligan et al., 1998). The declining SN number and increasing NS number is consistent with the change in the direction of the global solar field which is thought to decide the leading field of MCs (Crooker, 2000). The number of bipolar MCs (SN + NS) is relatively constant (23, 22, 15 during rise, maximum, and declining phases) as noted by others (Li and Luhmann, 2004; Huttunen et al., 2005; Echer et al., 2005), which probably arises from the opposite trends in the number of SN and NS clouds. The number of unipolar (FS + FN) MCs shows a slight decline (17, 12, 10) as a function of time. The global field changed around May 2002 when the polarity reversal was complete in both solar poles (Gopalswamy et al., 2003b), consistent with the prevalence of leading northward field in MCs in the declining phase.

4. MCs and geomagnetic storms

A white-light CME observed near the Sun may result in a shock, sheath, and MC at 1 AU. Thus it is possible that a CME can be GE due to the southward field in the sheath, even though the associated MC may not be GE. In order to make

Table 1
MC types and their geoeffectiveness

MC type	#MCs	#MCs with Dst(d)[a]	#SHs with Dst(d)[c]	Dst level in MC(SH)[e]				GE fraction
				h	m	l	h + m	MC(SH) (%)
SN	39	35(31)	36(8)	12(7)	10(4)	13(25)	22(11)	56(28)
FS	19	19(18)	16(1)	10(4)	6(4)	3(8)	16(8)	84(42)
NS	21	19(16)	18(5)	8(4)	6(4)	5(10)	14(8)	67(38)
FN	20	2(2)[b]	18(16)	0(8)	0(3)	2(7)	0(11)	0(55)
All	99	75(67)	88(30)[d]	30(23)	22(15)	23(50)	52(38)	53(38)[f]

[a]The number in parentheses indicates the number of cases with Dst in the MC interval equals or exceeds the sheath Dst value.
[b]The Dst values seem to be noise.
[c]The number in parentheses indicates the number of cases with Dst in the sheath interval equals or exceeds the MC Dst value.
[d]The number of sheaths (88) contributing to Dst exceeds the actual number of shock events because we have included 12-h intervals ahead of non-shock MCs for reference. None of these cases was geoeffective.
[e]h = high ($\mathrm{Dst} \leqslant -100$ nT); m = medium ($-100 < \mathrm{Dst} \leqslant -50$ nT); l = low ($\mathrm{Dst} > -50$ nT).
[f]The geoeffectiveness rate of MCs becomes 66% when FN MCs are excluded; 56% of the 68 shock-driving MCs were geoeffective due to sheath portion.

this distinction, we have considered the southward Bz and its contribution to the Dst in both the cloud and sheath portions. We consider the sheath or the cloud portion contributing to the Dst if there is a southward Bz in the portion concerned. If the Dst index $\leqslant -50$ nT in the cloud or sheath, that portion is considered GE. Sometimes both cloud and sheath portions are GE. If the Dst index is at the storm level during a sheath or cloud portion due to a southward Bz interval preceding that portion, we do not consider the sheath or cloud to be GE. This usually happens when Dst $\leqslant -50$ nT interval is due to the recovery of a preceding storm.

The effect of V_{CME}, V_{MC}, Bt, and Bz on Dst is shown in Fig. 5. The Dst–Bt ($r = -0.83$) and Dst–Bz ($r = -0.82$) correlations were high, the Dst–V_{CME} ($r = -0.44$) correlation was low, while Dst–V_{MC} correlation was intermediate ($r = -0.68$). The speed–magnetic field products ($\mathrm{Bt}V_{CME}$, $\mathrm{Bt}V_{MC}$, $-\mathrm{Bz}V_{CME}$, and $-\mathrm{Bz}V_{MC}$) also had very high correlation with Dst: $r \sim 0.76-0.91$, the Dst$-\mathrm{Bz}V_{MC}$ correlation being the highest ($r = 0.91$) in agreement with other studies (Wu and Lepping, 2005; Gonzalez and Echer, 2005). These combinations are related to the Akasofu (1981) epsilon parameter, which represents the Poynting flux that drives the geomagnetic storms. The strong correlation of Dst with the CME speed–MC field products has important implications for CME-based space weather forecasting because it takes at least half a day before the CME arrives at Earth.

4.1. MC structure and geoeffectiveness

Table 1 (column 2) shows the number of MCs contributing to the Dst index with the ones dominant compared to the sheaths in parentheses. Column 4 gives the number of sheaths contributing to the Dst index, with the ones dominant compared to the cloud portion in parentheses. Columns 5–7 give the number of MCs (or sheaths in parentheses) with high (h, $\mathrm{Dst} \leqslant -100$ nT), medium (m, $-100\,\mathrm{nT} < \mathrm{Dst} \leqslant -50$ nT), and low (l, $\mathrm{Dst} > -50$ nT) Dst values, respectively. Column 8 gives the number of GE (h + m) MCs (and sheath in parentheses). The last column gives the fraction of MCs (and sheaths in parentheses) that was GE. MC types that definitely contain BzS are GE (SN—56%, FS—84%, NS—67%); the FN MCs have no BzS and hence they are not GE (two FN MCs had a small negative Dst values during the cloud interval, but this seems to be noise fluctuation). The sheaths of 11 FN MCs were GE; this amounts to 55% (11 out of 20) of the FN MCs being GE, making them equally important for geoeffectiveness. The 55% can be broken down to 40% intense (eight cases) and 15% moderate storms (three cases). This is contradictory to Zhang et al. (2004) who concluded that FN MCs are predominantly associated with moderate storms.

In Table 1, we see that 30 intense (h) and 22 moderate (m) Dst intervals were due to MCs. If we exclude the 20 FN MCs, these correspond to GE rates of 38% and 28%, respectively, for h and m level storms. For sheath events, the corresponding GE rates are 34% (23 h intervals) and 22% (15 m

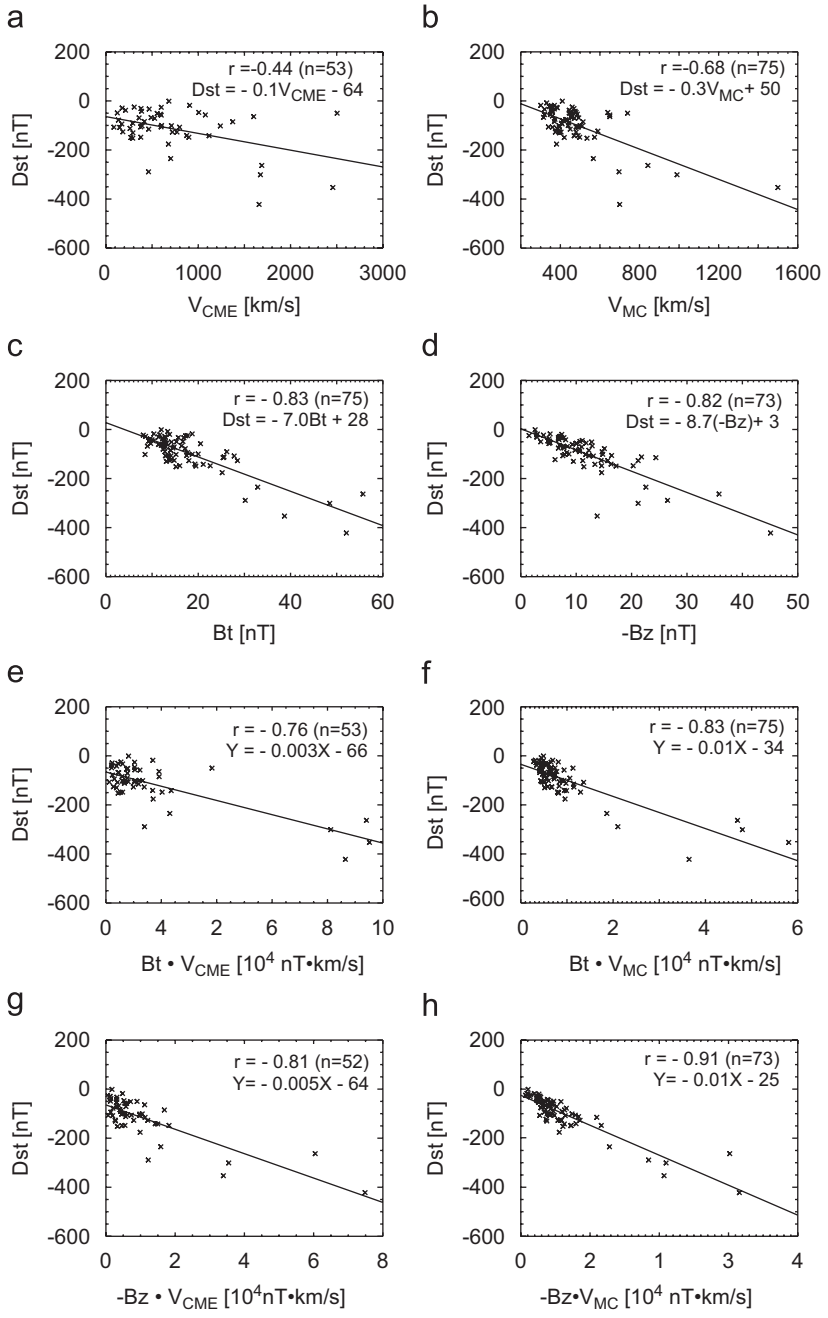

Fig. 5. Dst as a function of (a) CME speed, (b) MC speed, (c) Maximum field strength (Bt) in the MC, (d) Maximum BzS (i.e., Bz < 0), (e) BtV_{CME}, (f) BtV_{MC}, (g) BzV_{CME}, and (h) BzV_{MC}. FN MCs and those with no storm contribution from the MC are excluded in plots involving Bz. The correlation coefficients and the equations of the regression lines are given on the plots.

intervals). Table 1 shows that there were 53 h intervals, of which 30 (57%) were in the cloud and 23 (43%) in the sheath portions. The distribution was similar for m-level intervals: out of the 37 intervals with Dst $\leqslant -50$ nT, 22 (59%) were in the cloud and 15 (41%) were in the sheath portions. Overall, 53% of MC portions and 38% of sheaths were GE (see also Li and Luhmann, 2004). If we exclude the 20 FN MCs, the geoeffectiveness rate of MCs increases to 66%. It is not clear why more than half of the sheaths (55%) of the FN type MCs were GE, which is similar to the cloud portion of SN

Table 2
Geoeffective MCs and sheaths

MC type	SN	FS	NS	FN	Total
MC alone	14	8	8	0	30 (30%)
Sheath alone	3	0	2	11	16 (24%)
MC and sheath	8	8	6	0	22 (32%)
MC or sheath	25 (64%)	16 (84%)	16 (76%)	11 (55%)	68 (69%)

MCs (56%) but twice the geoeffectiveness rate of sheaths in SN MCs. Sheaths of other MC types were also GE, but to a lower degree: SN (28%), NS (38%), and FS (42%). This needs further investigation from the point of view of the MC origin at the Sun and IP propagation that might explain the polarity of the leading MC field and the sheath field (see, e.g., Crooker, 2000).

Table 2 lists the geoeffectiveness of MCs with various combinations: geoeffectiveness solely due to cloud portions, solely due to sheaths, due to both portions, and due to either portion. The overall geoeffectiveness of the MCs caused by either the cloud or the sheath portions is 69%. MCs are GE in 30 cases (or 30% of MCs) when their sheaths are not GE. Out of the 68 MCs with sheaths, the geoeffectiveness is solely due to sheaths in 16 cases (or 24%), while both the sheath and cloud portions are GE in 22 cases (or 32%). For individual MC types, the geoeffectiveness is similar to what is given in Table 1, but slightly higher for SN (64%) and NS (76%) MCs when "sheath alone" cases are included.

Over our study period, 88 well-defined intense ($Dst \leqslant -100$ nT) geomagnetic storms have been recorded[5] (Zhang et al., 2007). Of these, 13 were CIR-related storms. Forty three of the remaining 75 storms (or 57%) were due to MCs and the remaining 32 (or 43%) were due to NC ICMEs. The level of geoeffectiveness of MCs is thus similar to this work (see Tables 1 and 2) even though the starting point is different. For a smaller set of storms, Li and Luhmann (2004) found a slightly lower rate of association with MCs (46%).

Tables 1 and 2 also tell us that 31 MCs (or 33%) are not GE or only weakly GE ($Dst > -50$ nT) including the sheath portion. The non-GE MCs were generally lower in speed: the average speed (382 km/s) is well below that of all MCs (524 km/s). Only 10 non-GE MCs had speeds >400 km/s, and in most of these cases, the southward Bz had smaller values. The average Bz for the non-GE MCs is -5.2 nT, which is well below the average value (-9.4 nT) of all MCs. The product of low speed and low southward Bz is not expected to result in a significant storm as demonstrated in Fig. 5(h). Most of the non-GE MCs were from the rise phase (19 or 61%). The maximum phase had 10 (or 32%), while the declining phase had only 2 (7%).

[5]http://cdaw.gsfc.nasa.gov/geomag_cdaw/Data_master_table.

5. Discussion and conclusions

We have studied the solar source properties and geoeffectiveness of 99 MCs observed mostly during solar cycle 23. The large sample combined with the availability of data on CMEs remote-sensed when they are still near the Sun helped us obtain statistically significant results. We were able to obtain quantitative relationships between physical parameters of CMEs, MCs, and the Dst index. We have confirmed some of the results obtained from smaller sets of events. The results of this study can be summarized as follows: (1) The MC-associated CMEs are faster and wider on the average similar to the halo and GE CMEs. However, the average speed of MCs is only slightly greater than the slow solar wind speed at 1 AU because of the strong coupling between the solar wind and CMEs in the IP medium.

(2) The MC-associated CMEs originate from very close to the Sun center (within $\pm 30^\circ$ in longitude and latitude), and have a slight western bias (the average location is W07). CMEs with only shock signatures at Earth originated close to the solar limbs; CMEs associated with NC ICMEs originated at intermediate locations. Thus all ICMEs may be MCs if viewed from an appropriate vantage point. The deviations can be attributed to propagation effects that deflect the CMEs away from the Sun–Earth line.

(3) MC sources occur at higher heliographic latitudes during the rise phase compared to the maximum and declining phases, mimicking the butterfly diagram. This is true for all MC types. The butterfly diagram simply reflects the fact that the MC-producing regions are mostly active regions or the filament regions in the active region belts. The strong global dipolar field of the Sun may be channeling the CMEs toward the ecliptic so CMEs originating at higher latitudes are observed as MCs.

(4) SN MCs prevailed over NS MCs during cycle 23. The number of SN MCs declined from the rise phase to the declining phase, while the NS MCs had

the opposite trend. These trends are similar to other odd cycles.

(5) Two-thirds of all MCs were GE, similar to the frontside halo CMEs.

(6) The non-GE MCs are generally slow, have low magnetic field strengths, and occur mostly during the rise phase of the cycle.

(7) A large fraction (38%) of MCs had GE sheaths. The unusually high occurrence of GE sheaths (55%) in FN MCs makes them equally important for geoeffectiveness.

(8) The correlation of CME and MC speeds with MC magnetic field is confirmed for a much wider range of parameters.

(9) The Dst index is highly correlated with the total magnetic field and its southward component in the MCs, and moderately with the CME and MC speeds.

(10) Dst is highly correlated with the speed and magnetic field products. The V_{MC}–Bz correlation was the best ($r = 0.91$).

(11) The good $V_{CME}B-$Dst correlation may have a space weather application if one can estimate the magnetic field inside CMEs when they are near the Sun.

Acknowledgments

This work was supported by NASA SR&T and LWS TR&T programs. SOHO is a project of international cooperation between ESA and NASA. N.G. thanks the ISROSES organizers for travel support to the Varna meeting, where the results reported here were presented.

References

Akasofu, S.-I., 1981. Space Science Review 28 (2), 121–190.
Burlaga, L.F., et al., 1981. Journal of Geophysical Research 86, 6673–6684.
Crooker, N.U., 2000. Journal of Atmospheric and Solar-Terrestrial Physics 62, 1071–1085.
Echer, E., et al., 2005. Journal of Atmospheric and Solar-Terrestrial Physics 67, 839–852.
Gonzalez, W.D., Echer, E., 2005. Geophysical Research Letters 32, L18103.
Gonzalez, W.D., et al., 1998. Geophysical Research Letters 25 (7), 963–966.
Gopalswamy, N., 2006. Journal of Astrophysics and Astronomy 27 (2), 243–254.
Gopalswamy, N., et al., 2000. Advances in Space Research 25, 1851–1854.
Gopalswamy, N., et al., 2003a. Astrophysical Journal 586, 562–578.
Gopalswamy, N., et al., 2003b. Astrophysical Journal 598, L63–L66.
Gopalswamy, N., et al., 2005. Journal of Geophysical Research 110 (A9), A09S15.
Gopalswamy, N., et al., 2007. Journal of Geophysical Research 112 (A6), A06112.
Gosling, J.T., et al., 1991. Journal of Geophysical Research 96, 7831–7839.
Huttunen, K.E.J., et al., 2005. Annales Geophysicae 23 (2), 625–641.
Lepping, R.P., et al., 1995. Space Science Review 71, 207–229.
Lepping, R.P., et al., 2005. Annales Geophysicae 23 (7), 2687–2704.
Lepping, R.P., et al., 2006. Annales Geophysicae 24 (1), 215–245.
Li, Y., Luhmann, J., 2004. Journal of Atmospheric and Solar-Terrestrial Physics 66, 323–331.
Lindsay, G.M., et al., 1999. Journal of Geophysical Research 104 (A6), 12515–12523.
Loewe, C.A., Prölss, G.W., 1997. Journal of Geophysical Research 102 (A7), 14209–14213.
Mulligan, T., et al., 1998. Geophysical Research Letters 25 (15), 2959–2962.
Owens, M.J., et al., 2005. Journal of Geophysical Research 110, A01105.
Parker, E.N., 1957. Astrophysical Journal Supplement 3, 51–76.
Wu, C.-C., Lepping, R.P., 2005. Annales Geophysicae 24 (12), 3383–3389.
Yurchyshyn, V., et al., 2004. Space Weather 2, S02001.
Zhang, J., et al., 2004. Journal of Geophysical Research 109, A09101.
Zhang, J., et al., 2007. Journal of Geophysical Research 112 (A10), A10102.